JACS
JOURNAL OF THE AMERICAN CHEMICAL SOCIETY
Article
pubs.acs.org/JACS

Crystal Structures of Quinolinate Synthase in Complex with a Substrate Analogue, the Condensation Intermediate, and Substrate-Derived Product

Anne Volbeda,[†] Claudine Darnault,[†] Oriane Renoux,[†] Debora Reichmann,[‡] Patricia Amara,[†] Sandrine Ollagnier de Choudens,[‡] and Juan C. Fontecilla-Camps*[,†]

[†]Metalloproteins Unit, Institut de Biologie Structurale, CEA, CNRS, Université Grenoble-Alpes, 71, Avenue des Martyrs, 38044 Grenoble Cedex 9, France

[‡]CEA/DRF/BIG/CBM/BioCat, CNRS UMR 5249, LCBM, Université Grenoble Alpes, LCBM, Grenoble, France

Supporting Information

ABSTRACT: The enzyme NadA catalyzes the synthesis of quinolinic acid (QA), the precursor of the universal nicotinamide adenine dinucleotide (NAD) cofactor. Here, we report the crystal structures of complexes between the *Thermotoga maritima* (*Tm*) NadA K219R/Y107F variant and (i) the first intermediate (**W**) resulting from the condensation of dihydroxyacetone phosphate (DHAP) with iminoaspartate and (ii) the DHAP analogue and triose-phosphate isomerase inhibitor phosphoglycolohydroxamate (PGH). In addition, using the *Tm*NadA K219R/Y21F variant, we have reacted substrates and obtained a crystalline complex between this protein and the QA product. We also show that citrate can bind to both *Tm*NadA K219R and its Y21F variant. The **W** structure indicates that condensation causes dephosphorylation. We propose that catalysis by the K219R/Y107F variant is arrested at the **W** intermediate because the mutated protein is unable to catalyze its aldo−keto isomerization and/or cyclization that ultimately lead to QA formation. Intriguingly, PGH binds to NadA with its phosphate group at the site where the carboxylate groups of **W** also bind. Our results shed significant light on the mechanism of the reaction catalyzed by NadA.

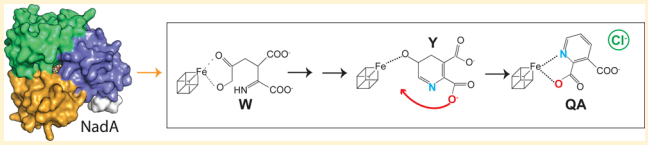

INTRODUCTION

Quinolinic acid (QA) is the precursor in the synthesis of the essential nicotinamide adenine dinucleotide (NAD(P)) cofactor by all organisms.[1] NAD is involved in many fundamental redox reactions through hydride transfer. Most prokaryotes synthesize this cofactor using the *de novo* II pathway that involves the condensation of iminoaspartate (IA) with a triose phosphate sugar.[2] IA is generated from L-Asp by the L-aspartate oxidase NadB in *Escherichia coli* and by aspartate dehydrogenase (NadB-II or NadX) in *Thermotoga maritima* (*Tm*) whereas the condensation reaction is catalyzed by the quinolinate synthase NadA in both microorganisms.[3−5] Although IA synthesis and the formation of NAD(P) from QA are well-understood, QA synthesis has not been fully elucidated.[4,6] Catalytic mechanisms have been proposed differing in the nature of the triose phosphate that reacts with IA, either glyceraldehyde-3-phosphate (G3-P) or dihydroxyacetone phosphate (DHAP), and at the point at which dephosphorylation occurs.[4,6] Recent biochemical studies have confirmed that DHAP is the NadA substrate[7] favoring dephosphorylation upon condensation (Scheme 1) at odds with a previous proposition that postulated Schiff base formation between G3-P and IA as the first step of the reaction[4] (Scheme S1).

The three-domain [4Fe-4S]-containing NadA is an extensively multifunctional enzyme.[8,9] It may carry out the transformation of IA to its enamine tautomer (as suggested by the fact that it can use the IA produced by combining oxaloacetate with ammonium ions[10]), the condensation of this tautomer with DHAP, the aldo−keto isomerization of the condensed intermediate, and two dehydration steps (Scheme 1). The first of these dehydration reactions takes place upon

Scheme 1. Proposed Mechanism for QA Synthesis by NadA[a]

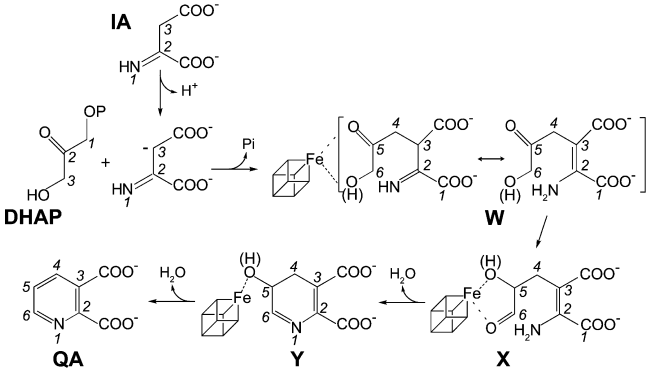

[a]This mechanism is based on the **W** complex (this study) and previous propositions (see text). Atoms are numbered according to IUPAC rules.

Received: June 8, 2016
Published: August 22, 2016

DOI: 10.1021/jacs.6b05884
J. Am. Chem. Soc. 2016, 138, 11802−11809

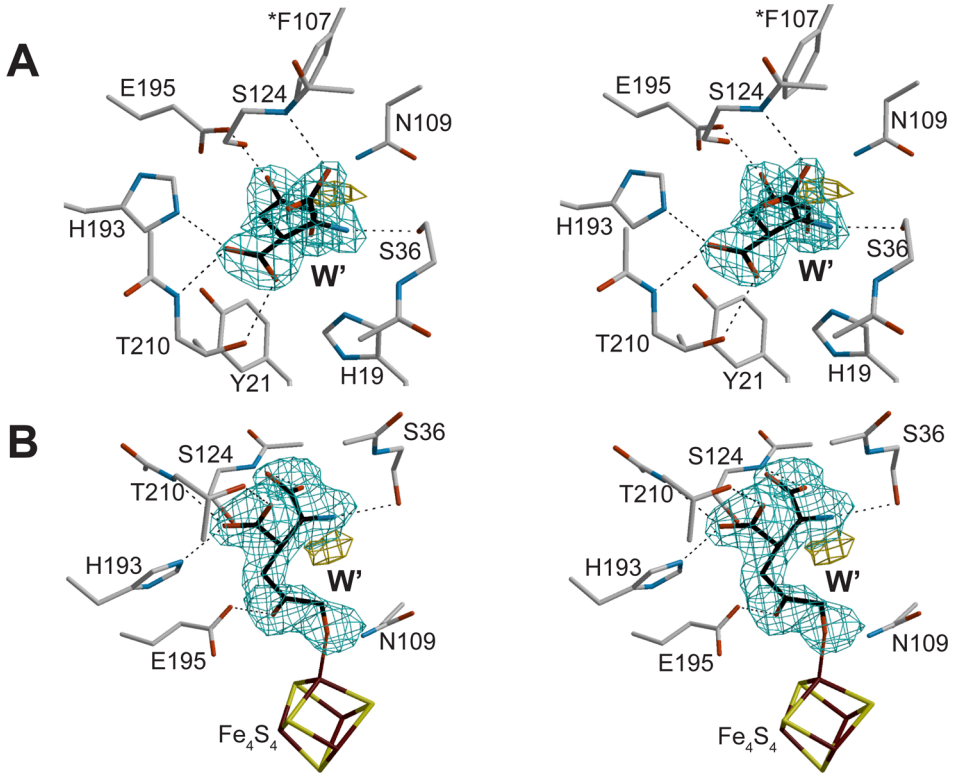

Figure 1. Stereoviews of the model and electron density "omit" map (blue mesh) of the *Tm*NadA complex with **W′**: 2-imino, 3-carboxy, 5-oxo, 6-hydroxy hexanoic acid. (A) Rotated by 90° about a horizontal axis relative to part B. Maps were contoured at 4.0σ and 3.0σ, respectively. When **W′** is included in the calculated structure factors and phases, there is a residual peak next to it (brown, contoured at 4σ) (see also Figure S1).

formation of a Schiff base and cyclization of the condensed intermediate whereas the second one is reminiscent of the reaction catalyzed by aconitase.[11] Indeed, like this hydratase/dehydratase, NadA coordinates a [4Fe-4S] cluster with three cysteine ligands, which leaves an iron ion with a site available for Lewis-type catalysis.[12] As shown by Mössbauer spectroscopy, this unique iron ion interacts with the thiol groups of the QA analogue and NadA inhibitor 4,5-dithiohydroxyphtalic acid (DTHPA).[13] This result showed that the iron−sulfur cluster is directly involved in catalysis.

The first published structure of a quinolinate synthase was the one from *Pyrococcus horikoshi* (*Ph*) devoid of its [4Fe-4S] cluster.[6] Nevertheless, the malate IA analogue was found bound to the protein yielding valuable information on the possible IA binding site in NadA. The also apo structure of *Pyrococcus furiosus* NadA, with one of its three domains rotated by 180°, was used to model a holo [4Fe-4S] cluster-containing protein and to propose the binding of substrates and the last **Y** intermediate of the reaction.[14] Subsequently, we determined the holo crystal structure of *Thermotoga maritima* (*Tm*) NadA K219R and confirmed the availability of the unique iron at the end of a long tunnel connecting the [4Fe-4S] cluster with the molecular surface.[12] We also proposed a mechanism for the second dehydration step that uses a deprotonated Tyr21 (*Tm* numbering used throughout).[12] Here, we report the crystal structures of complexes of the *Tm*NadA K219R/Y107F variant, which lacks QA synthetic activity (Table S1), with (i) the substrate-derived condensation product **W** (Scheme 1) at 1.9 Å resolution and (ii) the triose-phosphate isomerase (TIM) inhibitor phosphoglycolohydroxamate (PGH) at 1.45 Å resolution (Table S2). PGH, which closely resembles DHAP with only the substitution of C3 by N, is also an inhibitor of NadA from both *Tm* and *Escherichia coli* (*Ec*) (Table S1). In addition, we report a complex of the *Tm*NadA K219R/Y21F variant with substrate-derived QA at 1.9 Å resolution and complexes of the K219R and K219R/Y21F variants with citrate. The K219R variant is equivalent to the wild-type enzyme because the mutation has no incidence in the active site structure or in the enzymatic activity[12] (Table S1). Consequently, we will call, for simplicity, the single K219R variant *Tm*NadA* and the two double variants *Tm*NadA* Y107F and *Tm*NadA* Y21F; these two tyrosine residues belong to the NadA active site. We have also carried out a series of docking experiments that shed significant light on the active site structural rearrangements that take place during and after catalysis. While this paper was in preparation, Esakova et al. reported the structure of a complex of *Ph*NadA with soaked QA.[15] Also, during its revision an additional complex of *Ph*NadA with soaked QA and structures of this enzyme in a complex with DHAP and the IA analogue itaconate were reported.[16]

RESULTS AND DISCUSSION

Crystallization trials of the *Tm*NadA* Y107F variant, incubated overnight in the glovebox with DHAP, oxaloacetic acid, and ammonium ions[10] at neutral pH, were initially set at pH 8.5, a value that is optimal for NadA activity.[17] Under these conditions, crystals of *Tm*NadA* Y107F displayed a significant electron density peak at the active site in an omit $F_{obs} - F_{calc}$ map calculated with refined model phases (both in the presence and absence of citrate, used as either buffer or additive). It was possible to build the **W** condensation product (Scheme 1) into this density in two conformations: a major one called **W′** (Figure 1) and defined as 2-imino, 3-carboxy, 5-oxo, 6-hydroxy

DOI: 10.1021/jacs.6b05884
J. Am. Chem. Soc. 2016, 138, 11802−11809

hexanoic acid and a minor conformation **W″** that could correspond to either the same species or its 2-amino tautomer (Figure S1); the electron density does not provide a clear distinction between these two latter alternatives. The density does, however, clearly show that the condensation reaction took place prior to and/or during crystallization. Subsequent crystallization experiments of *Tm*NadA* Y107F in the absence of citrate and with substrates set up at the catalytically unfavorable pH 6.5[17] showed the active site to be devoid of the electron density peak described above (not shown). This result confirms that the electron density observed in *Tm*NadA* Y107F crystals grown at pH 8.5 with substrates corresponds to an enzyme-derived catalytic product.

W binds NadA mainly through its two carboxylate groups (sites I and II) and through its C6−O$^-$ to the unique iron ion of the [4Fe-4S] cluster (site III) (Figure 2).

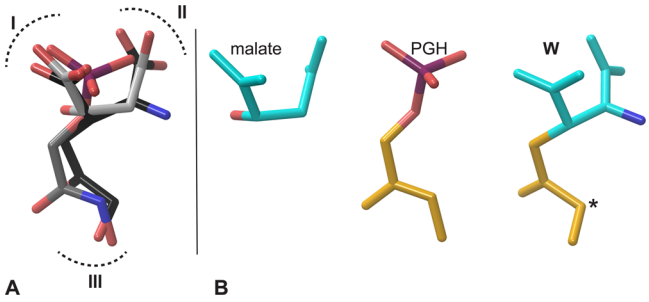

Figure 2. (A) Superposition of malate[6] (light gray C atoms), **W′** (black C atoms), and PGH (medium gray C atoms); phosphorus, oxygen, and nitrogen atoms are shown in purple, red, and blue, respectively. I, II, and III denote anchoring points of ligands to the NadA active site. (B) This figure shows how the top region of **W** binds to NadA like malate binds to *Ph*NadA[6] (light blue) and its bottom part like PGH does (orange). * indicates the C atom in **W** which corresponds to an N atom in PGH. A rotation of malate about a vertical 2-fold rotation axis would position its —OH group on top of the =NH of **W′** (see text and Soriano et al.[14]). Fenwick and Ealick have used their PGH-like DHAP and malate-like itaconate-*Ph*NadA complexes to propose a theoretical model for **W** that approximates our crystal structure.[16]

Crystals of the *Tm*NadA* Y107F PGH complex were obtained by incubating the enzyme overnight in the glovebox with the inhibitor. PGH binds with its phosphate group to site I and, partially, to site II, and it has its N−O$^-$ and keto group bound to the unique iron (site III) (Figures 2A and 3A). A comparison of the PGH and **W** structures shows that their Fe-binding modes are similar, the main differences being the following: (i) the orientation of PGH N, which is C6 in **W** (Figure 2), with N forming an H-bond with a solvent molecule (Figure 3A), and (ii) the distance of the keto O to the cluster unique iron (Figure S2C). As could be expected, DHAP binds to *Ph*NadA through the same three sites (Figure 1A in ref 16).

Although citrate did not interfere with **W** formation and binding at pH 8.5, it formed crystalline complexes with *Tm*NadA* at acidic pH in the presence of substrates and with its Y21F variant at basic pH in their absence (Figure 3B and Table S2). Citrate resembles **W** and binds the enzyme in a very similar way at sites I–III (Figure 2A). Interestingly, QA synthesis at pH 8.0 by *Ec*NadA was 4 times higher in 100 mM HEPES buffer than in 100 mM citrate−K_2HPO_4 buffer.[10] Using phosphate buffer alone, QA production was half that obtained

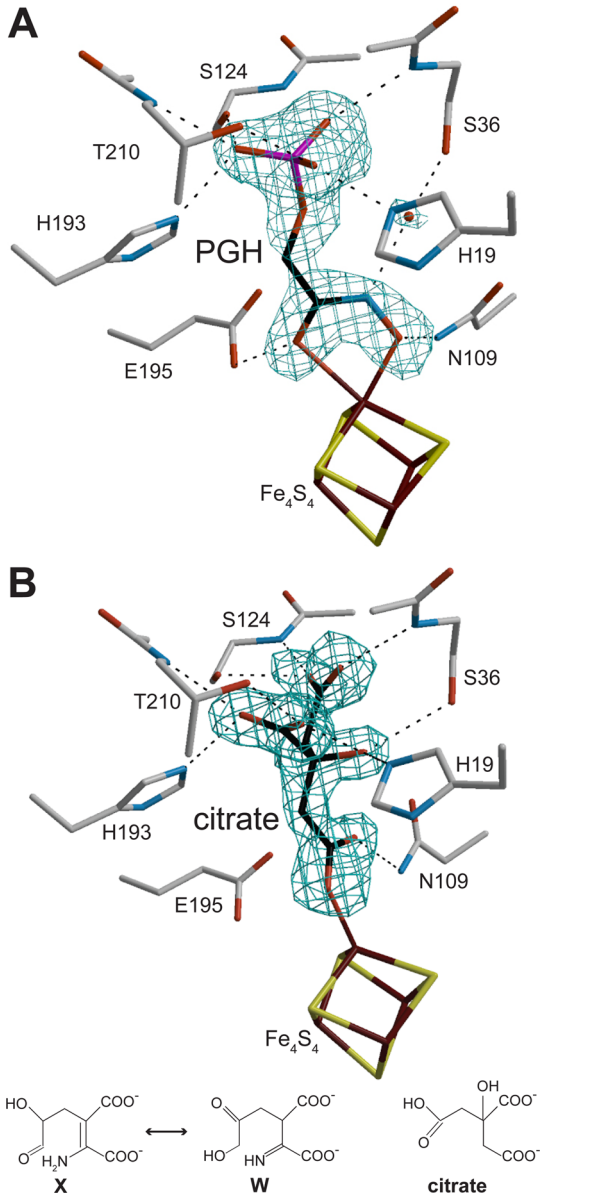

Figure 3. (A) Phosphoglycolohydroxamate (PGH) bound to *Tm*NadA* Y107F contoured at 3.3σ. (B, top) Model and electron density omit map contoured at 4.0σ for the citrate-bound *Tm*NadA* Y21F variant. (B, bottom) **X** and **W** on one hand and citrate on the other have similar structures.

with HEPES buffer. This shows partial inhibition of QA synthesis by both citrate and phosphate.

The crystal structure of the proposed **W** intermediate displays several of the features expected for a condensation product/reaction intermediate. First, its two carboxylate groups bind *Tm*NadA as malate does in the *P. horikoshi* structure[6] (Figure 2). Second, as indicated above, both the DHAP analogue PGH and **W** bind tightly to the unique iron of the [4Fe-4S] cluster with their terminal —O$^-$ atoms and to a lesser extent with their C=O groups (respectively, at d = 2.0 Å and d = 2.45 Å for PGH) (Figure 3A and Figure S2). This arrangement is supported by bond valence theory because, in general, a metal with + n valence forms a significantly stronger bond with a negatively charged alkoxide than with a neutral keto group.[18]

DOI: 10.1021/jacs.6b05884
J. Am. Chem. Soc. 2016, 138, 11802−11809

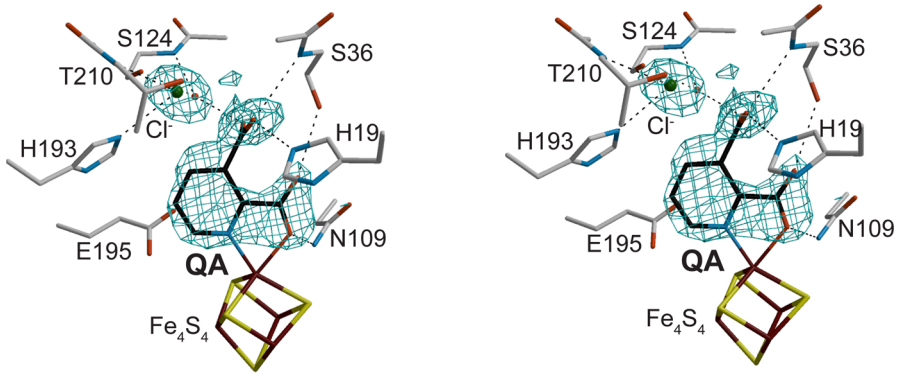

Figure 4. Stereoview of the model and electron density "omit" map (blue mesh) of a *Tm*NadA complex with QA (quinolinic acid) and a Cl^- ion (green sphere) contoured at 2.8σ.

Third, the structure of **W** (Figure 1) also shows that, as suggested by Nasu et al.,[19] Flint and Allen,[20] and Sakuraba et al.,[6] the condensation of IA with DHAP involves the *elimination of the phosphate group* of the latter. In this pathway, IA is expected to be deprotonated at C3 to become the nucleophile that attacks the C1 of DHAP (Scheme 1).[19,20] Fourth, the **W″** intermediate has its N atom well-oriented for its nucleophilic attack on C6 and subsequent Schiff base formation and cyclization (Figure S1).[3,20]

We have previously reported that the *Tm*NadA* Y21F variant has undetected QA synthetic activity after a short incubation period.[12] The same result was obtained by Esakova et al. with their equivalent *Ph*NadA Y23F variant.[15] We had also observed that the corresponding *Ec*NadA Y49F variant displays 7% activity showing that it was still able to produce QA.[12] In order to further explore the properties of the *Tm*NadA* Y21F variant, we collected 1.9 Å resolution X-ray data from a crystal grown from this protein incubated with substrates. Unexpectedly, in this crystal the enzyme has the QA product bound to the unique Fe ion of the [4Fe-4S] cluster in a bidentate mode (Figure 4). A similar configuration was found for QA when cocrystallized with *Ph*NadA.[15,16]

In order to clarify this point, we have now followed the kinetics of QA synthesis by the *Tm*NadA* Y21F variant in solution for a period similar to the one used to grow the crystals. Under these conditions, we observed QA synthesis with about 30% product formed relative to the control after 35 h (Figure 5). This result implies that the Y21F mutation renders the reaction very sluggish but still possible. Importantly, our proposed role for Tyr21 in the second deprotonation process[12] is consistent with this result.

The shortest path for the reorientation of QA after the second dehydration step (**Y** → QA in Scheme 1), with the least energy cost, corresponds to an approximate clockwise 100° rotation about an axis perpendicular to the ring plane and a 50° rotation about a vertical axis parallel to it (Figure 6). This movement is easy to rationalize because dehydration removes the remaining **Y** (hydr)oxo ligand of the unique Fe ion. We have also considered the possibility that **W** binds to *Tm*NadA* Y107F in a nonproductive way due to the tyrosine mutation. Because of the active site structure and expected role of the [4Fe-4S] cluster, one plausible alternative orientation for the condensation intermediate would result from an approximate 180° rotation of **W** about an axis going through a point equidistant between binding sites I and II and a point at site III. However, starting from that position, QA would have to cover a

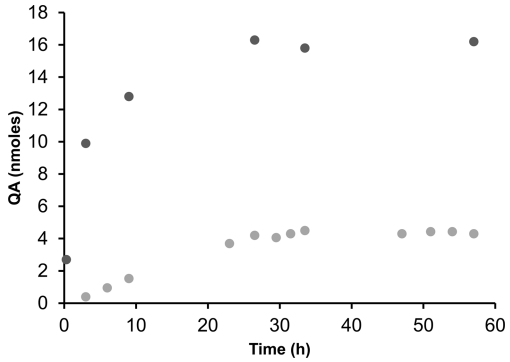

Figure 5. Activity of NadA proteins from *T. maritima*. The activities of *Tm*NadA* (dark gray circles) and *Tm*NadA* Y21F (light gray circles) (30 μM) were assayed inside the glovebox at 23 °C using DHAP, oxaloacetic acid, and ammonium sulfate as substrates. All reagents were used at concentrations and the temperature that mimicked the crystallization conditions except for the omission of the polyethylene glycol (PEG) precipitating agent: 2 mM DHAP, 10 mM oxaloacetic acid, 5 mM ammonium sulfate, in 125 mM Tris pH 7.2, 50 mM KCl buffer. *Tm*NadA* and *Tm*NadA* Y21F proteins were prepared as previously described.[12] The curves plateaued at about 5.5 QA molecules per enzyme molecule for *Tm*NadA* and 1.6 QA molecules per enzyme molecule for the *Tm*NadA* Y21F variant.

significantly longer path involving severe clashes with the protein in order to bind to the [4Fe-4S] cluster as observed (Figure 4 and Figure S4). In addition, our structural analyses indicate that there is a clear asymmetry between two opposite sides of the active site with residues facing the reactive **W** C2−N and C6 atoms being more flexible (Figure S5). Thus, Ser36, Tyr107, Asn109, and Ser124 adopt significantly different orientations in the various structures whereas His19, Tyr21, Glu195, and T210 display much lower structural variability. Given the complex series of reactions catalyzed by NadA, the observed asymmetric amino acid side chain flexibility, also evident in *Ph*NadA,[16] is likely to be a requirement for activity.

Because we observed significant concerted adjustments of the active site structure in our different complexes, we decided to explore how these changes determine the binding of intermediates and product using molecular docking (see Methods section). First, we docked QA in the *Tm*NadA* Y21F-QA X-ray model with and without the chloride ion included in the docking grid; the correct QA conformation (Figure 4) was recovered in both cases. Another pose with a similar score was obtained in the absence of Cl^-, where both QA carboxylate groups were bound to the unique iron of the

DOI: 10.1021/jacs.6b05884
J. Am. Chem. Soc. 2016, 138, 11802−11809

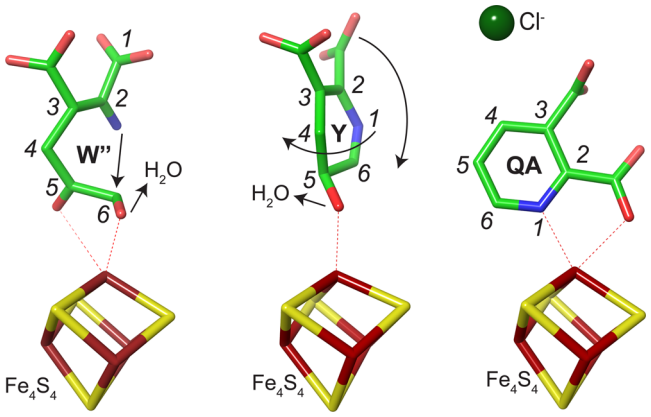

Figure 6. From left to right: X-ray structure of **W″** (Figure S1), docked model of **Y** in the citrate-bound form of the *Tm*NadA* structure without this ligand (see text and Methods section for details), and X-ray structure of QA (Figure 4). Left: the arrows represent (i) the nucleophilic attack of the N atom upon the C6 atom (after **X** is generated by aldo−keto isomerization, see Scheme 1) and (ii) the first dehydration reaction. Center: after the second dehydration that generates the final product, two rotations, indicated by curved arrows, are sufficient to obtain the observed bidentate QA binding mode. Right: in the QA structure, a modeled chloride ion (green sphere) approximately occupies one of the carboxylate group binding sites found in **W″**.

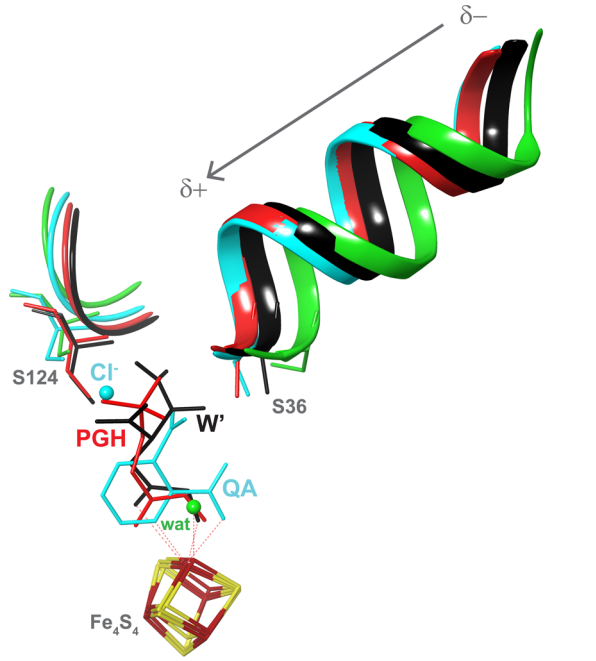

Figure 7. Ribbon representation of elements of Y107F-**W′** (in black), Y21F-QA (in cyan), Y107F-PGH (in red), and the previously published open uncomplexed *Tm*NadA*[12] (PDB code 4P3X) (in green). The helix consisting of residues 35−45 and the 123−126 loop are shown with the corresponding ligand at the active site; namely, **W′**, (QA + Cl^-), PGH, and a water molecule (same color for the helix, the loop, and the ligand(s) in each case). The [4Fe-4S] cluster is also depicted. The dipole moment of the helix points at the anion-binding (carboxylate groups) site (gray arrow).

[4Fe-4S] cluster. This result explains the presence of the Cl^- ion in the crystal structure that compensates for the loss of one carboxylate negative charge caused by QA binding to the cluster. Docking QA in the *Tm*NadA* structure (Table S2), with citrate removed, led to a pose where the two carboxylate groups of QA are positioned as in **W** and citrate (Figures 1 and 3B). This result is reminiscent of the *Ph*NadA-malate[6] and *Ph*NadA-itaconate structures[16] where the ligands do not bind a Fe/S cluster and may represent the QA orientation immediately after the second dehydration (Figure S4). We also found a pose that reproduces **W′** in its observed conformation (Figure 1) using the corresponding *Tm*NadA* Y107F X-ray structure. In contrast, this **W′** binding mode could not be obtained in the *Tm*NadA* Y21F-QA structure, with QA removed, because of a steric clash between Ser36 and the **W′**-imino group (Figure 7). We conclude that the way molecules bind to NadA is strongly dependent on small changes in the conformation of the active site residues and their loops within a confined space. In a previous study, we modeled a closed form of *Tm*NadA and manually docked the **Y** intermediate in it.[12] We have now used our high resolution crystal structures of the closed form of *Tm*NadA to dock **Y** in the *Tm*NadA*, with citrate removed. The highest scores corresponded to two poses that differ in their ring puckering.[12] The **Y** pose that most likely derives from **W″** (Figure S1) is shown in Figure 6 (center).

In conclusion, all of these observations reinforce our proposal that the **W** structure, most likely in its **W″** conformation, corresponds to the first intermediate in QA synthesis. In this orientation only two significant rotations are necessary to explain the positional changes in the **W** → **X** → **Y** → QA series of reactions (Figure 6, Figure S4, and Scheme 1).

We next sought to determine why, in the *Tm*NadA* Y107F variant, the reaction is stopped at the **W** condensation intermediate. We knew the problem did not arise from the conditions we used to carry out the reaction and crystallization because they were identical to those employed with the *Tm*NadA* Y21F variant that yielded QA. A comparison of the *Tm*NadA* Y107F variant structure with the *Ph*NadA-DHAP X-ray model[16] shows that the absence of the Tyr107 −OH group in the Phe107 variant modifies the orientation of its side chain and causes a rotation of that of Ser124. Positioning Tyr107 and Ser124 of *Tm*NadA* Y107F as found in *Ph*NadA-DHAP generates putative short hydrogen bonds (SHB) between these two residues and between Tyr107 and Glu195. In addition, this acidic residue forms another SHB with the keto group of **W** (Figure 8). The tight interaction between Tyr107 and Glu195, absent in our Y107F variant, is likely to change the pK_a of Glu195 which, in turn, may modify its reactivity toward **W**. This effect would explain why the Tyr107 −OH group is *functionally* essential. Like PGH, we note that **W** in the *Tm*NadA* Y107F variant still has a C6 terminal alkoxide group implying that aldo−keto isomerization has not taken place. This isomerization reaction is essential because, after IA condenses with DHAP,[7,17] Schiff base formation and cyclization to yield **Y** from **X** requires a C6 terminal aldehyde (Scheme 1). We propose that the removal of the −OH group in the Y107F variant has rendered *Tm*NadA incapable of catalyzing the aldo−keto isomerization, a process that involves acid−base catalysis and probably requires a SHB between Tyr107 and Glu195. Another possible reason for the lack of activity of the *Tm*NadA* Y107F variant, hinted at by the very recent report by Fenwick and Ealick,[16] is that the carbonyl and alkoxide ligands to the unique iron, but not the rest of **W**, may have nonproductive positions due to the absence of the Tyr107 −OH group. However, this possibility is not obvious because our PGH structure has the same iron ligand orientation as **W**

DOI: 10.1021/jacs.6b05884
J. Am. Chem. Soc. 2016, 138, 11802−11809

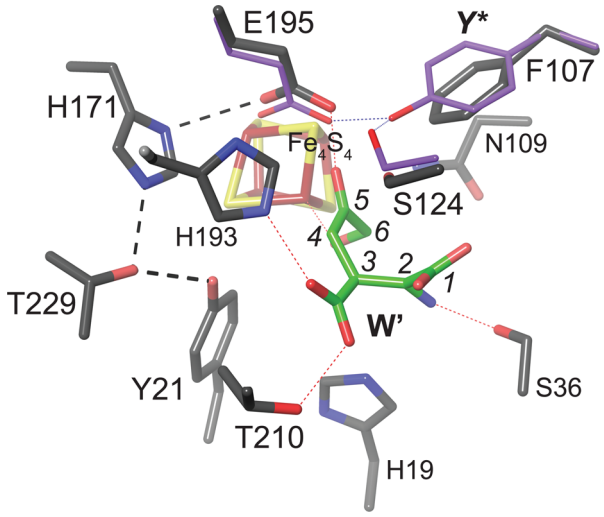

Figure 8. Interactions at the active site. Thick black dashed lines indicate hydrogen bonds sequentially linking residues Tyr21, Thr229, His171, Glu195 in our X-ray model. Thin red dashed lines show interactions of active site residues with the bound **W′** condensation product. For residues Phe107, Ser124, and Glu195, we have included their counterparts in the *Ph*NadA DHAP complex structure (light purple side chain carbon atoms). Thin blue dashed lines depict short hydrogen bonds involving **Y*** in that model.[16] See Figure S3 for a stereoview depiction of this figure.

and the hydroxyl O atom of the modeled Tyr107 (Figure 8) would be at about 5 Å from the nearest PGH atom (Figure S2C).

In our previous study,[12] when Glu228 from *E. coli* NadA, which corresponds to Glu195 in *Tm,* was mutated to Ala, there was a 20-fold drop in QA synthetic activity. We then postulated that Glu195, along with Thr229 and His171, is part of a catalytic triad that deprotonates Tyr21, which then extracts a proton from C4 of the **Y** intermediate yielding QA (Scheme 1).[12] Now we propose that Glu195 is also properly positioned to participate in the aldo−keto isomerization reaction (Figure 8). We note that the reported intrinsic NadA TIM activity[7] cannot operate on **W** because it does not significantly depend on the presence of the [4Fe-4S] cluster, which is essential for NadA conformational integrity and **W** binding.

Examination of **W′** shows that the modeled imino N atom, although positioned on the same side as the C6 atom, might not be correctly oriented to attack it, as required to form the Schiff base (Figure 1 and Scheme 1). Conversely, the N atom of the alternative **W″** would be correctly oriented and at the right distance from C6 (Figure S1). We also note that Tyr21, the triad mentioned above, Tyr107, and Ser124 should form an arc of sequentially hydrogen-bonded side chains at the NadA active site region (Figure 8). This arrangement, including the short Tyr107-Glu195 interaction, is likely to be instrumental for proton transfer processes during catalysis.

Explaining the condensation reaction (DHAP + IA → **W** in Scheme 1) is complicated by the fact that both the phosphate group of the DHAP analogue PGH and the carboxylate moieties of **W** (and malate[6] and itaconate[16]) bind to the same site in NadA. If PGH and DHAP[16] share their binding mode and IA binds like malate does in *Ph*NadA, one of the two substrates will have to displace the other for the condensation to occur at the [4Fe-4S] cluster-containing active site. One possibility, suggested by the *Tm*NadA* Y107F structures with bound **W** and PGH (Figure 1, Figure S1, and Figure 3A, respectively), is that DHAP binds first, like PGH, to the [4Fe-4S] cluster with its phosphate group partially occupying the site where the two carboxylate moieties of the IA analogues malate and itaconate bind in the *P. horikoshi* NadA structure.[6,16] In this case, IA would have to displace it during or after the reaction. The phosphate group could then sit close to Tyr21, His193, and His171, residue types known to be favorable for its binding.[21] However, this displacement would imply rather extensive conformational changes of these residues and their loops, which cannot be reliably modeled at this time.

An alternative mechanism might be possible in which the condensation reaction takes place at the *Tm*NadA tunnel,[12] close to the molecular surface, with the resulting **W** product migrating and binding to the [4Fe-4S] cluster as found in our structure (Figure 1). A comparison of the uncomplexed *Tm*NadA* (open form),[12] the *Tm*NadA* Y107F variant in complex with **W′**, and the *Tm*NadA* Y21F variant in complex with QA shows that several movements condition the access to the active site region, especially those of the 35−45 α-helix and the 123−126 loop that respond to the nature of a bound molecule or its absence. Thus, a shift of the 35−45 α-helix, due to its dipole moment, helps to close the tunnel leading to the active site cavity upon either carboxylate (**W′**) or phosphate (PGH) binding (Figure 7). We had already noticed this difference when comparing our uncomplexed *Tm*NadA structure with the one from malate-bound *Pyrococcus horikoshi.*[12] This, in turn, suggests that conformational changes at or near the buried [4Fe-4S] cluster/active site are fundamental for catalysis. The opening of NadA to lodge both substrates with its subsequent closing after dephosphorylation has been also proposed while this paper was being revised.[16] We will further explore this possibility using both functional and theoretical approaches.

■ CONCLUSION

In summary, the *Tm*NadA* Y107F-**W** crystal structure provides direct evidence for the following: (i) Condensation of IA with DHAP is coupled to dephosphorylation, and at odds with a previous inference,[15] it can be catalyzed by the Y107F variant. (ii) Glu195 is likely to be directly involved in the aldo−keto isomerization of **W″** to **X**. Our results also predict, based on the **W″** structure, that **X** will be well-poised to undergo Schiff base formation, dehydration, and cyclization to form **Y**. After the second dehydration, which our results strongly suggest is helped by Tyr21 (Figure 5), the QA product rotates inside the NadA active site forming a bidentate complex with the unique Fe ion of the [4Fe-4S] cluster. Whichever mechanism is responsible for its release from NadA is most likely related to the remarkable malleability of the buried active site and its access tunnel. Despite being buried, a series of NadA active site residues display a flexibility that optimizes their interactions with reactants and product at the active site. Taken together, our results strongly suggest that, at odds with previous conclusions,[16,19] this site is fine-tuned to participate in every one of the reactions required to synthesize QA from IA and DHAP.

■ METHODS

Protein Expression and Purification of *Thermotoga maritima* (*Tm*) NadA* Y107F. The Y107F mutation was introduced into the *nadA* gene from *Tm* using pT7-tmnadAK219RHis as template[12] and the QuikChange site-directed mutagenesis kit. The oligonucleotides

DOI: 10.1021/jacs.6b05884
J. Am. Chem. Soc. 2016, 138, 11802−11809

used as mutagenic primers were P1 (5′-cggtggttctcttcgtgaacagt-3′) and P2 (5′-actgttcacgaagagaaccaccg-3′), and the corresponding plasmid was named pT7-tmnadAY107FHis. The plasmid was entirely sequenced to ensure that no error was introduced during the PCR reaction. Expression, purification, and chemical reconstitution of *Tm*NadA* Y107F was performed as described previously for *Tm*NadA*.[12] After reconstitution, the measured ratios of iron and sulfur atoms per protein monomer were: 4.5 Fe and 4.9 S for *Tm*NadA* Y107F, 3.3 Fe and 4.1 S for *Tm*NadA*, and 2.5 Fe and 3.5 S for *Tm*NadA* Y21F.

Protein Analysis. Protein concentration was measured by the method of Bradford[22] using bovine serum albumin as a standard and applying correction factors for NadA as previously described.[12] Protein-bound iron was determined under reducing conditions with bathophenanthroline disulfonate after acid denaturation of the protein, and labile sulfide was determined by the method of Beinert.[23,24] UV−vis spectra were recorded with a Cary 1 Bio (Varian) spectrophotometer.

***Tm*NadA Enzymatic Activity.** *Tm*NadA enzymatic activity was assayed at 45 °C in the presence of 2 mM DHAP and 10 mM ammonium sulfate and 5 mM oxaloacetate as iminoaspartate (IA) precursors.[12] The *Tm*NadA concentration used was 30 μM. The same conditions, except that the temperature was 37 °C, were used for the *Escherichia coli* enzyme (Table S1).

Protein Crystallization. *TmNadA* Y107F-W Complex.* A 100 μL portion of a solution containing 20 mg/mL (0.58 mM) of protein in 125 mM Tris HCl pH 7.2 50 mM KCl was incubated anaerobically overnight at 20 °C with 1 μL of 0.5 M ammonium sulfate, 2 μL of 0.5 M oxaloacetic acid, and 4 μL 50 mM dihydroxyacetone phosphate. Hanging drops were set by mixing 1 μL of the incubated solution with 1 μL of a solution containing 22% (w/v) PEG3350, 100 mM Tris base, pH 8.5, and either 200 mM sodium citrate or 100 mM $LiSO_4$. The drops were anaerobically equilibrated against 1 mL of one of the latter solutions at 20 °C. Crystals grew as thin plates after 1 week. The plates were mounted in cryo-loops and flashed-cooled in liquid propane inside a glovebox after having soaked them in a cryo-protecting solution containing 40% (w/v) PEG3350, 100 mM Tris base, pH 8.8, and either 200 mM sodium citrate or 100 mM $LiSO_4$.

TmNadA Y107F-PGH Complex.* A 100 μL portion of a solution containing 20 mg/mL (0.58 mM) of protein in 125 mM Tris HCl pH 7.2 50 mM KCl was incubated anaerobically overnight with a 2:1 molar ratio of phosphoglycolohydroxamate (PGH) corresponding to 7 μL of a 20 mM solution. Hanging drops were set by mixing 1 μL of the incubated solution with 1 μL of a solution containing 18% (w/v) PEG3350, 100 mM Tris base, pH 9.0, and 100 mM $LiSO_4$. The drops were anaerobically equilibrated against 1 mL of the latter solution at 20 °C. Crystals grew as thin plates after 10−12 weeks. The plates were mounted in cryo-loops and flash-cooled in liquid ethane inside a glovebox after having soaked them in a cryo-protecting solution containing 40% (w/v) PEG3350, 100 mM Tris base, pH 8.8, and 100 mM $LiSO_4$.

TmNadA-Citrate Complex.* A 100 μL portion of a solution containing 20 mg/mL (0.58 mM) of protein in 125 mM Tris HCl and 50 mM KCl at pH 7.2 was incubated anaerobically overnight with 2.8 μL of a solution containing 50 mM of the inhibitor PGA (giving a 2:1 molar ratio of PGA to protein). Hanging drops were next prepared by mixing 1 μL of the incubated solution with 1 μL of crystallization solution containing 30% (w/v) PEG4000, 50 mM NaCl, 100 mM NH_4 acetate, and 100 mM Na citrate pH 5.4. The drops were anaerobically equilibrated against 1 mL of the latter solution at 20 °C. Crystals grew as thin plates after 2 weeks. They were mounted in cryo-loops and flash-cooled in liquid propane inside a glovebox after being soaked in a cryo-protecting solution corresponding to the crystallization solution after increasing the PEG4000 concentration to 40% (w/v).

TmNadA Y21F-Citrate Complex.* A 100 μL portion of a solution containing 20 mg/mL (0.58 mM) of protein in 125 mM Tris HCl pH 7.2 50 mM KCl was incubated anaerobically overnight at 20 °C with 2.8 μL of 0.05 M DHAP (giving a 2:1 molar ratio of DHAP to protein). Hanging drops were set by mixing 1 μL of the incubated solution with 1 μL of a solution containing 28% (w/v) PEG3350, 100 mM Bis Tris propane, pH 8.5, and 100 mM sodium citrate. The drops were anaerobically equilibrated as above. Crystals grew as thin plates after 3 days. The crystals were mounted in cryo-loops and flashed-cooled in liquid propane inside a glovebox after having soaked them in a cryo-protecting solution containing 40% (w/v) PEG3350, 100 mM Bis Tris propane, pH 8.3, and 100 mM sodium citrate.

TmNadA Y21F-QA complex.* A 100 μL of a solution containing 20 mg/mL (0.58 mM) of protein in 125 mM Tris HCl pH 7.2 50 mM KCl was incubated anaerobically overnight at 20 °C with 1 μL of 0.5 M ammonium sulfate, 2 μL of 0.5 M oxaloacetic acid, and 4 μL 50 mM dihydroxyacetone phosphate. Hanging drops were set by mixing 1 μL of the incubated solution with 1 μL of a solution containing 26% (w/v) PEG3350, 100 mM Bis Tris propane, pH 8.0, and 100 mM NaCl. The drops were anaerobically equilibrated as above. Crystals grew as thin plates after 1 week. The crystals were mounted in cryo-loops and flashed-cooled in liquid propane inside a glovebox after having soaked them in a cryo-protecting solution containing 38% (w/v) PEG3350, 100 mM Bis Tris propane, pH 8.0, and 100 mM sodium chloride.

X-ray Data Collection and Structure Determination. All X-ray diffraction data for the $P2_1$ monoclinic crystals were collected on a Pilatus detector, using ID (insertion device) beamlines of the European Synchrotron Radiation Facility (ESRF) in Grenoble, except *Tm*NadA* Y21F-QA, which was collected at the ESRF beamline BM30A on an ADSC Quantum 315r detector (Table S2). After indexation, integration, and initial scaling of the collected data with the *XDS* package,[25] a final scaling and merging step was performed with the *AIMLESS* program[26] of the *CCP4* package.[27] The structures of the different enzyme complexes were solved by molecular replacement[28] starting from the known *Tm*NadA structure in a different crystal form.[12] Atomic positions and temperature (*B*-) factors were next refined with the program *REFMAC5*[29] using anisotropic *B*-factors for all models except *Tm*NadA* Y107F-**W** and *Tm*NadA* Y21F-QA for which isotropic *B*-factors were refined along with TLS parameters. Hydrogen atoms were included in their riding positions in all refinements. Local manual model corrections were performed with *COOT*.[30] A new dictionary (cif) file was developed for the refinement of the **W** intermediate, using 109.5° bond angles for sp^3 carbons involved in single bonds and 120° angles for sp^2 carbon, nitrogen, and oxygen atoms involved in double bonds (see Scheme 1). The Protein Data Bank (PDB) ID codes for these structures are 5F3D, 5LQS, 5F33, 5LQM, and 5F35.

Molecular Docking. Molecular docking was performed with the program Glide (version 7.0) from the Schrödinger Suite.[31] Hydrogen atoms were added to the *Tm*NadA* Y21F-QA, *Tm*NadA* Y107F-**W**, and *Tm*NadA* citrate-containing X-ray models (see Protein Crystallography section). Protonation states were assigned as in the standard protein preparation protocol in the Schrödinger suite. Model geometries were energy minimized with a maximum root-mean-square deviation of 0.3 Å to avoid a large deviation from the original X-ray models. Water molecules in both models were removed. The receptor docking grids were defined using the location of **W**, QA, and citrate in the crystal structures of *Tm*NadA* Y21F-QA, Y107F-**W** and citrate complexes, respectively, to define the active site cavities in both grids. The QA, **W′**, and **Y** molecules were prepared using the program Ligprep (version 3.7)[31] (with addition of hydrogen atoms and generation of stereoisomers whenever applicable).

■ ASSOCIATED CONTENT

Supporting Information

The Supporting Information is available free of charge on the ACS Publications website at DOI: 10.1021/jacs.6b05884.

Specific quinolinate synthase activity of NadA proteins from *T. maritima* and *E. coli*, X-ray data and refinement statistics, alternative mechanism for QA synthesis, and further analyses of *Tm*NadA complex crystal structures (PDF)

DOI: 10.1021/jacs.6b05884
J. Am. Chem. Soc. 2016, 138, 11802−11809

AUTHOR INFORMATION

Corresponding Author

*juan.fontecilla@ibs.fr

Notes

The authors declare no competing financial interest.

ACKNOWLEDGMENTS

We thank the CEA and the CNRS for institutional support. Part of this work used the platforms of the Grenoble Instruct center (ISBG; UMS 3518 CNRS-CEA-UJF-EMBL) with support from FRISBI (ANR-10-INSB-05-02) within the Grenoble Partnership for Structural Biology (PSB). We appreciate the help from the staff of the ESRF beamlines and the computing facility provided by the Commissariat à l'Energie Atomique (CEA/DSV/GIPSI), Saclay, France, and the Centre de Calcul Recherche et Technologie (CEA/CCRT). We thank the Agence Nationale pour la Recherche for Contract ANR-12-BS07-0018-01 (NADBIO). S.O.d.C. also acknowledges partial financial support from the ARCANE Labex (ANR-11-LABX-0003−01), and J.C.F.-C. also thanks the Direction des Sciences du Vivant du CEA for financial support by the BioEnergie program.

REFERENCES

(1) Foster, J. W.; Moat, A. G. *Microbiol. Rev.* **1980**, *44*, 83.
(2) Gerdes, S. Y.; Scholle, M. D.; D'Souza, M.; Bernal, A.; Baev, M. V.; Farrell, M.; Kurnasov, O. V.; Daugherty, M. D.; Mseeh, F.; Polanuyer, B. M.; Campbell, J. W.; Anantha, S.; Shatalin, K. Y.; Chowdhury, S. A.; Fonstein, M. Y.; Osterman, A. L. *J. Bacteriol.* **2002**, *184*, 4555.
(3) Nasu, S.; Wicks, F. D.; Sakakibara, S.; Gholson, R. K. *Biochem. Biophys. Res. Commun.* **1978**, *84*, 928.
(4) Begley, T. P.; Kinsland, C.; Mehl, R. A.; Osterman, A.; Dorrestein, P. *Vitam. Horm.* **2001**, *61*, 103.
(5) Yang, Z.; Savchenko, A.; Yakunin, A. F.; Zhang, R.; Edwards, A. M.; Arrowsmith, C. H.; Tong, L. *J. Biol. Chem.* **2003**, *278*, 8804.
(6) Sakuraba, H.; Tsuge, H.; Yoneda, K.; Katunuma, N.; Ohshima, T. *J. Biol. Chem.* **2005**, *280*, 26645.
(7) Reichmann, D.; Couté, Y.; Ollagnier de Choudens, S. *Biochemistry* **2015**, *54*, 6443.
(8) Ollagnier de Choudens, S.; Loiseau, L.; Sanakis, Y.; Barras, F.; Fontecave, M. *FEBS Lett.* **2005**, *579*, 3737.
(9) Cicchillo, R. M.; Tu, L.; Stromberg, J. A.; Hoffart, L. M.; Krebs, C.; Booker, S. J. *J. Am. Chem. Soc.* **2005**, *127*, 7310.
(10) Nasu, S.; Gholson, R. K. *Biochem. Biophys. Res. Commun.* **1981**, *101*, 533.
(11) Beinert, H.; Kennedy, M. C.; Stout, C. D. *Chem. Rev.* **1996**, *96*, 2335.
(12) Cherrier, M. V.; Chan, A.; Darnault, C.; Reichmann, D.; Amara, P.; Ollagnier de Choudens, S.; Fontecilla-Camps, J. C. *J. Am. Chem. Soc.* **2014**, *136*, 5253.
(13) Chan, A.; Clémancey, M.; Mouesca, J. M.; Amara, P.; Hamelin, O.; Latour, J. M.; Ollagnier de Choudens, S. *Angew. Chem., Int. Ed.* **2012**, *51*, 7711.
(14) Soriano, E. V.; Zhang, Y.; Colabroy, K. L.; Sanders, J. M.; Settembre, E. C.; Dorrestein, P. C.; Begley, T. P.; Ealick, S. E. *Acta Crystallogr., Sect. D: Biol. Crystallogr.* **2013**, *69*, 1685.
(15) Esakova, O. A.; Silakov, A.; Grove, T. L.; Saunders, A. H.; McLaughlin, M. I.; Yennawar, N. H.; Booker, S. J. *J. Am. Chem. Soc.* **2016**, *138*, 7224.
(16) Fenwick, M. K.; Ealick, S. E. *Biochemistry* **2016**, *55*, 4135.
(17) Suzuki, N.; Carlson, J.; Griffith, G.; Gholson, R. K. *Biochim. Biophys. Acta, Gen. Subj.* **1973**, *304*, 309.
(18) Tranchemontagne, D. J.; Mendoza-Cortés, J. L.; O'Keeffe, M.; Yaghi, O. M. *Chem. Soc. Rev.* **2009**, *38*, 1257.
(19) Nasu, S.; Wicks, F. D.; Gholson, R. K. *J. Biol. Chem.* **1982**, *257*, 626.
(20) Flint, D. H.; Allen, R. M. *Chem. Rev.* **1996**, *96*, 2315.
(21) Copley, R. R.; Barton, G. J. *J. Mol. Biol.* **1994**, *242*, 321.
(22) Bradford, M. M. *Anal. Biochem.* **1976**, *72*, 248.
(23) Beinert, H. *Anal. Biochem.* **1983**, *131*, 373.
(24) Fish, W. W. *Methods Enzymol.* **1988**, *158*, 357.
(25) Kabsch, W. *Acta Crystallogr., Sect. D: Biol. Crystallogr.* **2010**, *66*, 125.
(26) Evans, P. R.; Murshudov, G. N. *Acta Crystallogr., Sect. D: Biol. Crystallogr.* **2013**, *69*, 1204.
(27) Winn, M. D.; Ballard, C. C.; Cowtan, K. D.; Dodson, E. J.; Emsley, P.; Evans, P. R.; Keegan, R. M.; Krissinel, E. B.; Leslie, A. G.; McCoy, A.; McNicholas, S. J.; Murshudov, G. N.; Pannu, N. S.; Potterton, E. A.; Powell, H. R.; Read, R. J.; Vagin, A.; Wilson, K. S. *Acta Crystallogr., Sect. D: Biol. Crystallogr.* **2011**, *67*, 235.
(28) McCoy, A. J.; Grosse-Kunstleve, R. W.; Adams, P. D.; Winn, M. D.; Storoni, L. C.; Read, R. J. *J. Appl. Crystallogr.* **2007**, *40*, 658.
(29) Murshudov, G. N.; Skubak, P.; Lebedev, A. A.; Pannu, N. S.; Steiner, R. A.; Nicholls, R. A.; Winn, M. D.; Long, F.; Vagin, A. A. *Acta Crystallogr., Sect. D: Biol. Crystallogr.* **2011**, *67*, 355.
(30) Emsley, P.; Lohkamp, B.; Scott, W. G.; Cowtan, K. *Acta Crystallogr., Sect. D: Biol. Crystallogr.* **2010**, *66*, 486.
(31) Schrödinger, LLC: New York, NY, 2016.

DOI: 10.1021/jacs.6b05884
J. Am. Chem. Soc. 2016, 138, 11802−11809